

Visualizable Delivery of Nanodisc Antigen-Conjugated Adjuvant for Cancer Immunotherapy

Yangyun Wang^{1†}, Subin Lin^{2†}, Hanqiu Jiang³, Yuan Gu¹, Yanxian Wu¹, Jie Ma¹, Yubin Ke³, Leshuai W. Zhang¹, Yong Wang^{1*} & Mingyuan Gao^{1,4*}

¹State Key Laboratory of Radiation Medicine and Protection, School of Radiation Medicine and Protection, Collaborative Innovation Center of Radiation Medicine of Jiangsu Higher Education Institutions, Soochow University, Suzhou 215123, ²Department of Orthopedic, The Second Affiliated Hospital of Soochow University, Suzhou 215004, ³China Spallation Neutron Source, Dongguan Branch, Institute of High Energy Physics, Chinese Academy of Sciences, Dongguan 523803, ⁴Institute of Chemistry, Chinese Academy of Sciences, Beijing 100190

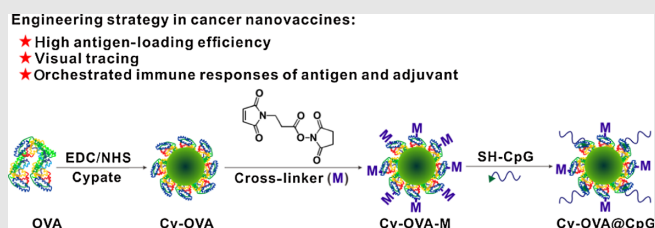
*Corresponding authors: wangyongac@gmail.com; gaomy@iccas.ac.cn; †Y. Wang and S. Lin contributed equally to this work.

Cite this: *CCS Chem.* **2022**, 4, 1238–1250

DOI: 10.31635/ccschem.021.202000670

Engineering synthetic vaccines is promising for improving the efficacy of cancer immunotherapy. One of the major challenges in the development of vaccines is achieving controllable codelivery of antigen and adjuvant to lymph nodes for maximizing the antitumor immune responses. To address this issue, we herein developed an innovative visualizable nanodisc vaccine based on ovalbumin (OVA) and short-stranded oligodeoxynucleotides containing unmethylated cytosine-phosphate-guanine (CpG) motifs. The nanovaccine was fabricated by covalently attaching CpG onto the surface of a nanodisc antigen formed upon self-assembly of amphiphilic molecular conjugates of OVA and cypate (Cy), a near-infrared (NIR) fluorescent dye, for noninvasively visualizing the delivery of the resulting nanovaccines. Systematic *in vitro* experiments demonstrated that the engineered nanovaccines can specifically locate to dendritic cells (DCs) via toll-like receptor 9 and membrane thiols, and then

efficiently activate DCs. The animal experiments combining NIR fluorescence imaging with the lymphatic T-cell phenotype and key cytokine secretion analyses revealed that targeted lymphatic homing of the mature DCs and consequent priming of CD8⁺ T cells were enabled to initiate strong tumor-specific T-cell responses with robust immune memory effects. Thus, this study offers a visualizable platform for optimizing the efficacy of nanovaccines toward cancer immunotherapies.



Keywords: nanovaccines, DC activation, *in vivo* trafficking, visualization, immunotherapy

Introduction

Vaccines hold enormous potential to stimulate systemic immune responses in cancer immunotherapy, but the response rate of clinical vaccines is unfortunately <30%.¹

The challenge of vaccine development is not only achieving controllable codelivery of antigen and adjuvant to lymph nodes (LNs),² but also maximizing the functions of the two major components of a given vaccine by spatiotemporally manipulating their immunoregulatory

DOI: 10.31635/ccschem.021.202000670

Corrected Citation: *CCS Chem.* **2022**, 4, 1238–1250

Previous Citation: *CCS Chem.* **2021**, 3, 1328–1340

Link to VoR: <https://doi.org/10.31635/ccschem.021.202000670>

pathways.^{3,4} Because of the attenuated immune effects of traditional adjuvants such as aluminum salts and water-oil emulsions, new adjuvant formulations are being developed for engineering synthetic vaccines.^{5,6} As a potent molecular adjuvant, short-stranded oligodeoxynucleotides containing unmethylated cytosine-phosphate-guanine (CpG) motifs can considerably enhance antigen-specific immune responses by binding to toll-like receptor 9 (TLR9) in antigen-presenting cells (APCs).^{7,8} Nonetheless, small-molecule CpG-based vaccines have not fully realized clinical applications.⁹ Nanomaterials, including polymers,¹⁰⁻¹² lipid,^{13,14} silica,¹⁵ and gold nanomaterials,¹⁶ can provide an alternative carrier for the fabrication of nanovaccines and codelivering the antigen and CpG to draining LNs. These current nanovaccines attempt to activate APCs in the draining LNs,¹⁷ but the nonconjugated components in these nanovaccines also drain into the systemic circulation and access APCs in distal tissues, which might cause serious systemic toxicity.¹⁸ Hence, well-defined molecular structure and payload will be attractive for improving the LNs-targeting delivery and biosafety of nanovaccines.¹⁹

Moreover, the *in vivo* fate and function of vaccines after their delivery can also determine whether they can finally effectively prime cancer-specific cytotoxic CD8⁺ T cells.²⁰ Current predictors of vaccine efficacy, which are invasive and take months to develop, usually depend on the host response.^{21,22} The gap between administration and evaluation may lead to potential pathogen infection before verifying vaccine prevention.²³ Advanced bioimaging technology opportunely provides powerful tools to non-invasively visualize the *in vivo* spatiotemporal fate of administrated vaccines.²⁴ It is believed that visualizable delivery of vaccines is desirable to evaluate the efficacy of candidate formulations and improve their rationality of design for both preclinical and translational studies.²⁵ Therefore, in combination with the design of nanovaccines with precise targeting and optimal responses, there is an increasing need to integrate imaging functions in nanovaccines to understand how they will activate immune response and prevent tumors *in vivo*.^{26,27}

Herein, we report a novel ovalbumin (OVA)/CpG-based nanovaccine for cancer immunotherapy. The nanovaccine is comprised of a nanodisc antigen core formed upon self-assembly of amphiphilic conjugates of OVA and near-infrared (NIR) fluorescent dye cypate (Cy), and a shell of CpG molecules covalently attached on the surface of the core. The resulting nanovaccine, denoted as Cy-OVA@CpG, is characterized by high antigen-loading efficiency, small size (approximately 30 nm), adjustable ratio between antigen and adjuvant, and visualizability *in vivo*. The engineering nanovaccines can specifically deliver to dendritic cells (DCs) via the TLR9 and membrane thiols, and then efficiently activate DCs. Owing to the inherent NIR fluorescence, the spatiotemporal trafficking, particularly the accumulation of the nanovaccines in sentinel LNs, was noninvasively

monitored *in vivo* after delivery. Systematic animal experiments were then carried out to show the robust tumor-specific T-cell responses induced by the nanovaccines and the corresponding mechanisms.

Experimental Section

General procedure for nanoantigen and nanovaccines synthesis

The nanoantigen was synthesized according to the dye-induced assembly strategy of antigen molecules.²⁸ A 50 mL OVA solution (10 mg mL⁻¹, pH = 10) was added into 5 mL of 20 mM cypate sulfo-NHS (NHS = *N*-hydroxysulfosuccinimide). Sulfhydrylation stirring (500 rpm) for 24 h, the solution was dialyzed (8000–14,000 MW) against ultrapure water for 48 h. To synthesize the nanovaccines based on the nanoantigen (Cy-OVA), nanoantigen (0.4 μmol) was initially conjugated with *N*-succinimidyl 3-maleimidopropionate (0.8 μmol) to produce maleimide-grafted nanoantigen (Cy-OVA-M), and then the 3'-end sulfhydrylation CpG (5-TCCATGACGTTCCCTGACGTT-3) was reduced with tri(2-carboxyethyl) phosphine hydrochloride; the molar ratio was 1:10. Reduced CpG (12 nmol) was finally reacted with the Cy-OVA-M for the preparation of the nanovaccines. The quantitation of conjugated CpG was monitored with the Cy5.5-labeled CpG. The concentration of the obtained nanoantigen and nanovaccines was calculated with the absorbance performance of the Cy molecule. The morphology, structure, and hydrodynamic diameter were characterized by transmission electron microscopy (TEM), small-angle neutron scattering (SANS), and dynamic light scattering (DLS), respectively. More details are available in the [Supporting Information](#).

Animals and cells

All animal experiments were approved by the Animal Ethics Committee of Soochow University (Suzhou, China). This study was performed in strict accordance with the national guidelines for the care and use of laboratory animals (Certificate no. 20020008, Grade II) in the Soochow University Laboratory Animal Center (Suzhou, China). C57/BL6 and BALB/c mice were obtained from Suzhou JOINN Clinical Co., Ltd. (Suzhou, China). The orthotopic osteosarcoma model was established using 4-week-old female BALB/c mice based on the literature. All animal experiments were performed under anesthesia with 2.5% isoflurane. B16F10-OVA⁺ cells were kindly provided by Professor Xueguang Zhang at Soochow University. K7M2 cells were obtained from National Infrastructure of Cell Line Resource of China (Chinese Academy of Medical Sciences and Peking Union Medical College, Beijing, China). Cells were cultured in minimum essential medium [MEM, 10% fetal bovine

serum, 100 U/mL penicillin G sodium and 100 µg/mL streptomycin, MEM sodium pyruvate (1 mM), NaHCO₃, MEM vitamins, MEM nonessential amino acids, and 20 µM β-mercaptoethanol]. More details are available in the [Supporting Information](#).

Results and Discussion

Preparation and characterization of nanovaccines

The conjugate of Cy and OVA was initially prepared by covalently linking carboxylated Cy to OVA molecule via amidation reaction mediated by EDC and sulfo-NHS (EDC = *N*-(3-dimethylaminopropyl)-*N'*-ethylcarbodiimide). Owing to the hydrophobicity of the Cy dye, the resulting conjugates are amphiphilic and tend to self-assemble in aqueous systems into nanodisc with OVA-rich surface structures. Therefore, the resulting nanoparticles are also called nanoantigens and are subsequently denoted as Cy-OVA. Then, the thiolated CpG molecules were covalently attached via a sulfosuccinimidyl 4-(*N*-maleimidomethyl)cyclohexane-1-carboxylate (Sulfo-SMCC) linker to the surface of the nanoantigens,²⁹ as shown in Figure 1a, to form a quasi-core-shell-structured nanovaccine with both antigen and adjuvant simultaneously accessible, while the NIR dye molecules are embedded deep inside. According to the TEM results (Figures 1b and 1c), the average size of the resulting Cy-OVA@CpG nanovaccines is 18.9 ± 5.3 nm. The hydrodynamic size of the nanovaccines is approximately 27 nm as determined by DLS (Figure 1d), and the zeta potential is approximately -26.7 mV. SANS studies suggest that Cy-OVA@CpG particles possess a core-shell structure with an overall disc-like shape (Figure 1e), similar to the high-density lipoprotein-based nanovaccines previously reported.¹³ According to the SANS fitting results, the mean diameter is 28.2 nm, and the shell thickness is around 1.2 nm. To further characterize the resulting nanovaccines, Cy5.5-labeled CpG was prepared and used to construct a control vaccine for quantitatively estimating the coupling efficiency of CpG with UV-vis absorbance spectroscopy and fluorescence spectroscopy. As Figure 1f shows, the absorbance of Cy-OVA@CpG-Cy5.5 ranging from 550 to 850 nm is dramatically increased, showing the major characteristic of the absorption of Cy5.5, in comparison with Cy-OVA. The fluorescence spectroscopy results (Figure 1g) also support an effective coupling of CpG molecules onto the surface of the nanoantigen core, with a coupling efficiency up to 78% (Supporting Information Figure S1) and antigen to CpG ratio up to 15:1. Given that any possible cytotoxicity of the nanovaccines may impair the immunomodulatory effects,³⁰ they were evaluated *in vitro* for effects on cell viability. The cell survival rate results (Supporting Information Figure S2) suggest that the current

nanovaccines hardly affect the viability of mouse embryonic fibroblasts (3T3 cells) and DCs.

Target and activation of DCs *in vitro*

In the current design, the Cy-OVA@CpG nanovaccines are expected to specifically target the DCs via TLR9 and cell surface thiol moieties.^{12,31} To show such ability, DCs incubated with the nanovaccines were subjected to analyses with flow cytometry and confocal microscopy. According to the flow cytometry results in Figure 2a, the DCs' uptake of the Cy-OVA nanoantigens is 13.7%. However, it is as high as 70.0% for CpG labeled with Cy5.5, and further increases to 80.4% for the Cy-OVA@CpG nanovaccines. The remarkably high uptake of the nanovaccines by DCs can reasonably be attributed mainly to TLR9-mediated endocytosis and partially to the generally enhanced cellular uptake for nano-objects. Confocal microscopy results in Figure 2b also confirm that the DCs' uptake of Cy-OVA@CpG is much higher than that for Cy-OVA. In addition, the nanovaccines present relatively uniform signals across the cytoplasm of the DCs.

According to the current nanovaccine design, the surface maleimide groups of the nanoantigen particles have two functions. Some of them are used to covalently attach CpG molecules to form the nanovaccines and the remaining maleimide groups are expected to enhance the binding affinity of the nanovaccines to DCs through the cell surface thiol residues.^{32,33} As Figure 2c demonstrates, the DCs incubated with the Cy-OVA nanoantigens bearing surface maleimide groups (denoted as Cy-OVA-M) exhibit comparable fluorescence with those incubated with Cy-OVA@CpG nanovaccines, and they both show stronger fluorescence than the cells incubated with the nanoantigen particles (i.e., Cy-OVA), suggesting that CpG and the remaining maleimide residues on the surface of Cy-OVA@CpG nanovaccines synergistically enhance the specific codelivery of the antigen and adjuvant into the DCs.

In addition to effective DC targeting, the following activation of DCs is another key issue for priming immune response. To show the DC activation effect of the nanovaccines, flow cytometry and the Meso Scale Discovery (MSD) multiplex assay were carried out to analyze the change of DC phenotype and the release of different types of cytokines. Three phenotypic markers, including CD40, CD80, and CD86, were selected for showing DCs' maturation upon coincubation with Cy-OVA@CpG. Although both Cy-OVA nanoantigens and CpG adjuvant can stimulate DC maturation (Supporting Information Figures S3a-S3f), the DCs incubated with Cy-OVA@CpG present the highest activation level. After incubation with the nanovaccines for 24 h, the expressions of all three phenotypic markers in DCs increased by factors of 2-3 in comparison with those of the nontreated controls. Four proinflammatory cytokines secreted by mature DCs, including IL-1β, IL-6, TNF-α, and IL-12p70, were also

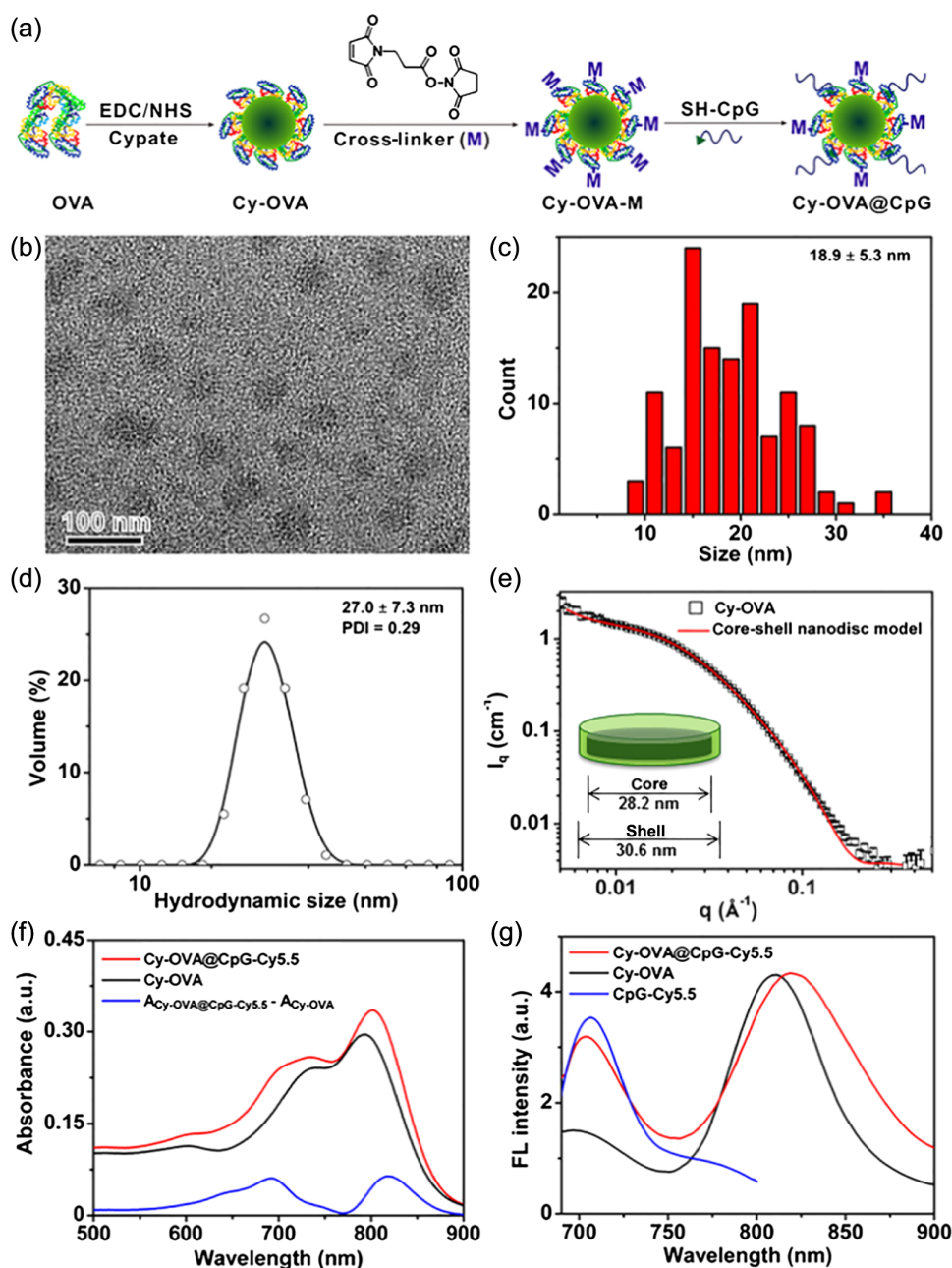


Figure 1 | Preparation and characterization of nanovaccines. (a) The fabrication strategy of nanovaccines. (b) The TEM image of Cy-OVA@CpG. (c) Size distribution of nanovaccines from TEM image. (d) The hydrodynamic size of Cy-OVA@CpG. (e) SANS and fitting model of Cy-OVA. (f) The absorbance spectra of Cy-OVA@CpG-Cy5.5 and Cy-OVA. (g) The fluorescence spectra of Cy-OVA@CpG-Cy5.5, Cy-OVA, and CpG-Cy5.5.

quantitatively determined. According to the secretion levels of these cytokines in Supporting Information Figure S3g, the CpG adjuvant group shows higher activation ability than the Cy-OVA nanoantigens. This may be due to the excellent phagocytosis and immune activation properties of CpG. Nonetheless, the DCs incubated with Cy-OVA@CpG generate much higher levels of cytokines than those treated with CpG, showing enhancement factors of 1.53, 1.28, and 1.49, for IL-12p70, IL-6, and TNF- α , respectively. With respect to IL-1 β , the

enhancement factor reaches as high as 3.6. All above results suggest that the Cy-OVA@CpG nanovaccines can specifically target, induce maturation, and enhance proinflammatory cytokines secretion of DCs.

Antigen presentation and hypermobility of DCs

To investigate the antigen presentation ability of DCs upon stimulation with Cy-OVA@CpG nanovaccines in

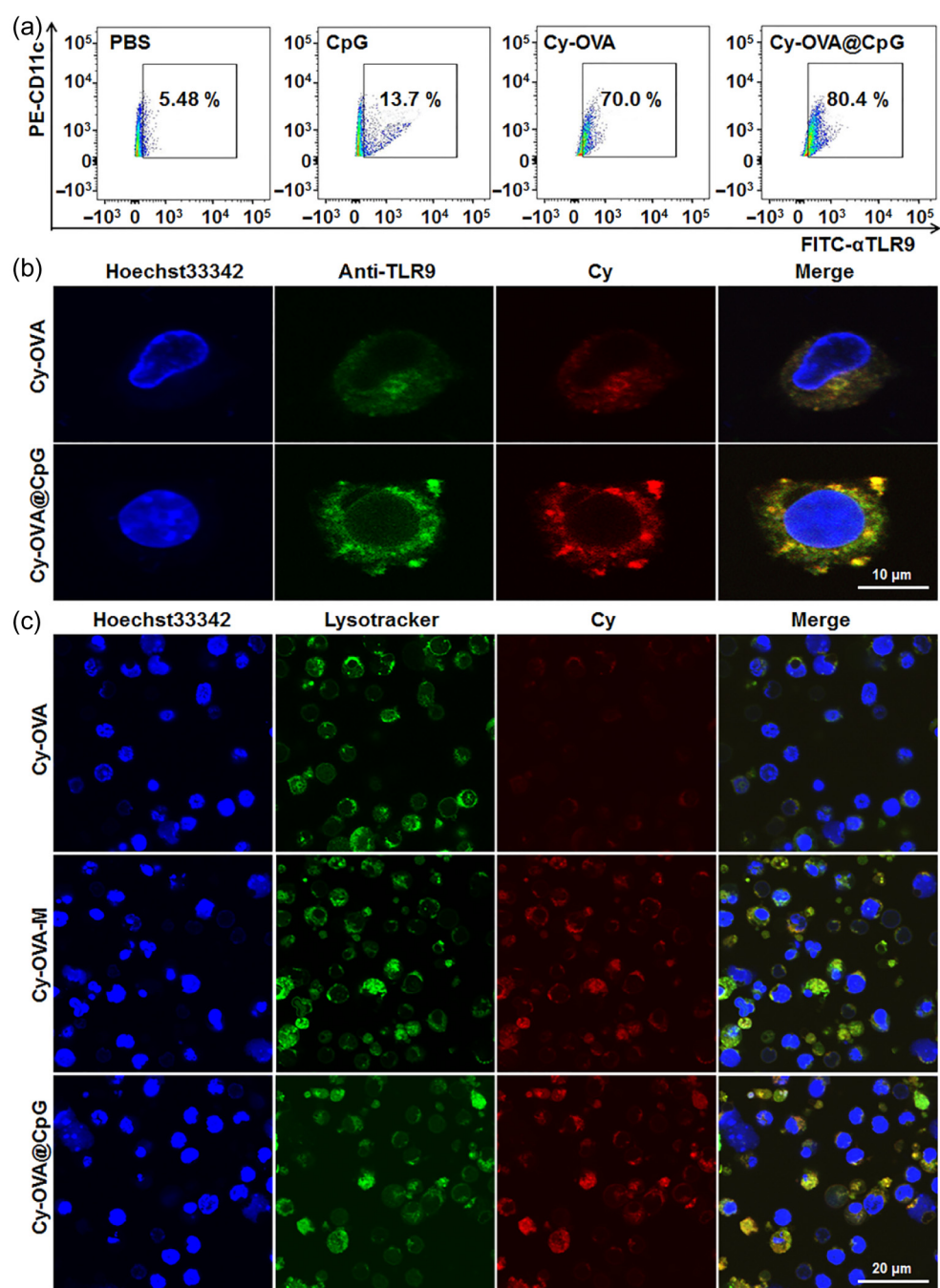


Figure 2 | Uptake pathway of DCs. (a) Flow cytometry for TLR9-directed targeted delivery. (b) Confocal microscopy for TLR9-directed targeted delivery. (c) Confocal microscopy for thiol on the DCs surface and TLR9-directed targeted delivery.

vitro, the expression of epitope-determining peptide (SIINFEKL) was assayed by flow cytometry. The SIINFEKL level is the highest for Cy-OVA@CpG stimulated DCs (Supporting Information Figure S4a). Although Cy-OVA also exhibits a remarkable effect, the adjuvant and antigen apparently synergistically enhance the antigen presentation.

The migration ability of mature DCs is very important for DCs homing to LNs to initiate adaptive immune

responses.²³ Once DCs become mature upon stimulation with antigen and adjuvant, they will upregulate the expression of biomarkers associated with the migration ability, such as CC-chemokine receptor 7 (CCR7). CCR7 enables DCs to migrate to and retain in regional LNs to expand the adaptive immune response.^{34,35} Therefore, CCR7 is considered an important biomarker for evaluating the migration ability of mature DCs. As shown in Supporting Information Figure S4b, the percentage of

DCs expressing CCR7 is 22.8% upon incubation with Cy-OVA@CpG, while it is only 5.7% and 18.6% for DCs incubated with free CpG and Cy-OVA, respectively. Apart from CCR7, the dynamics of the cytoskeleton are another indispensable indicator for DC motility.³⁶ As the two major components of cytoskeleton, microfilaments and microtubules were analyzed via immunofluorescence assays. The results given in Supporting Information Figure S4c reveal that the DCs incubated with Cy-OVA@CpG nanovaccines exhibit a typical motility phenotype showing strong signals from filamentous actin and extended veils, in contrast to those in the control groups that show weak filament-based phenotype. Regarding β -tubulin, no significant difference is shown among different groups of DCs incubated with CpG, Cy-OVA, and Cy-OVA@CpG, respectively. These results indicate that Cy-OVA@CpG nanovaccines can significantly enhance the motility of DCs, which is very conducive to the homing of mature DCs to the secondary lymphatic system.

In vivo lymphatic homing and immune responses

Timely and efficient delivery of vaccines to the secondary lymphatic system, for example, spleen and LNs, is essential for inducing strong and continuous immune responses against tumors.² Therefore, the NIR Cy dye was embedded in the nanovaccines to allow for real-time tracking of the migration and estimating of the LNs' retention of the current nanovaccines in vivo.²⁵ NIR fluorescence imaging studies were carried out after subcutaneously injecting Cy-OVA@CpG into the foot paws of mice, with the Cy-OVA nanoantigens serving as control. Figure 3a reveals that the lymphatic homing of both nanovaccine and its control can be visualized well. But the axillary and inguinal nodes of mouse receiving Cy-OVA@CpG nanovaccines present much stronger NIR fluorescence signals than those of the control. Moreover, these signals last for more than 6 days, suggesting that the Cy-OVA@CpG nanovaccines have potential for providing long humoral and cellular immune responses. The spatiotemporal dynamics of mature DCs stimulated by vaccines, particularly in terms of DCs' movement from peripheral tissues to the draining LNs, will be very important for regulating the DC-driven immune responses and vaccination.²¹ For DC-based vaccines, their continuous retention in the secondary lymphatic system can be attributed to the uptake and transport of the vaccines by DCs. Therefore, to demonstrate that DCs become mature and gain homing ability upon stimulation by the current nanovaccines in vivo, DCs were incubated with Cy-OVA@CpG nanovaccine prior to the subcutaneous foot paw injection, as shown in Figure 3b. The results in Figure 3c show that the DCs treated with Cy-OVA@CpG not only migrate to the inguinal LNs, but also accumulate

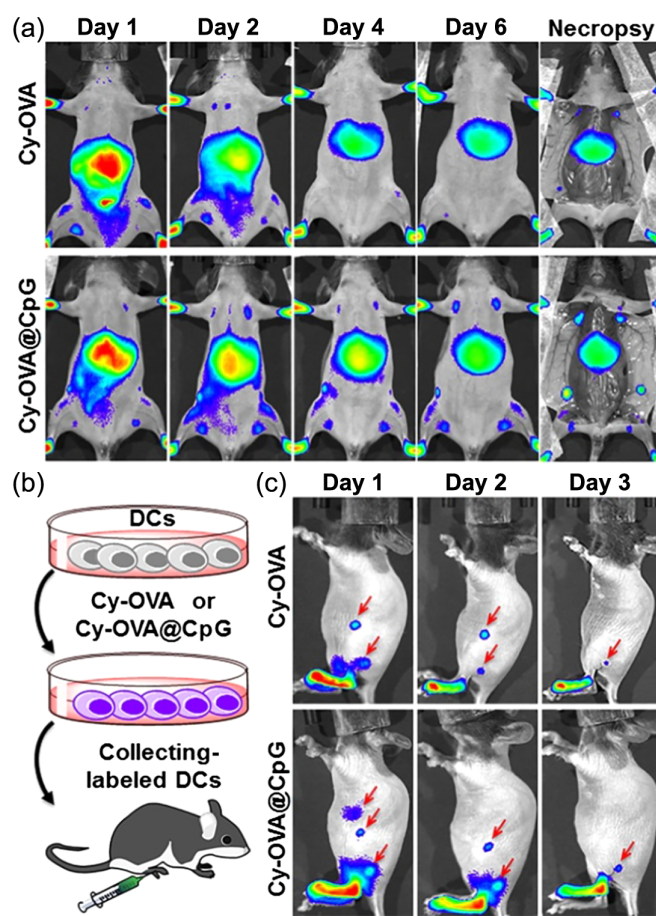


Figure 3 | (a) *In vivo* real-time NIR fluorescence tracking of Cy-OVA and Cy-OVA@CpG in the LNs for 6 days. The fluorescence imaging of necropsy was performed after 6 days. (b) Schematic diagram of DCs-incubated with Cy-OVA and Cy-OVA@CpG prior to the subcutaneous foot paw injection. (c) The dynamic migration over 3 days of DCs-loaded with Cy-OVA and Cy-OVA@CpG using *in vivo* NIR fluorescence imaging.

in the axillary LNs and spleen of mice 24 h postinjection of the DCs loaded with the nanovaccines. Moreover, the signals of inguinal LNs and axillary LNs are much stronger than those of the control mice receiving DCs loaded with Cy-OVA. Apart from that, the signal of the axillary LNs remains strong even 3 days postinjection. All these results indicate that the Cy-OVA@CpG nanovaccine is more conducive than the corresponding nanoantigen in promoting the DCs' migration to the secondary lymphatic system, quite probably in consequence of a series of positively regulated events, including chemotaxis, cytoskeletal rearrangement, and hypermobility.

After showing the positive effects of the nanovaccines, a series of immune responses caused by Cy-OVA@CpG homing to the secondary lymphatic system was then investigated by injection of the nanovaccines into the tail root (Figure 4a). Both Cy-OVA@CpG and its control,

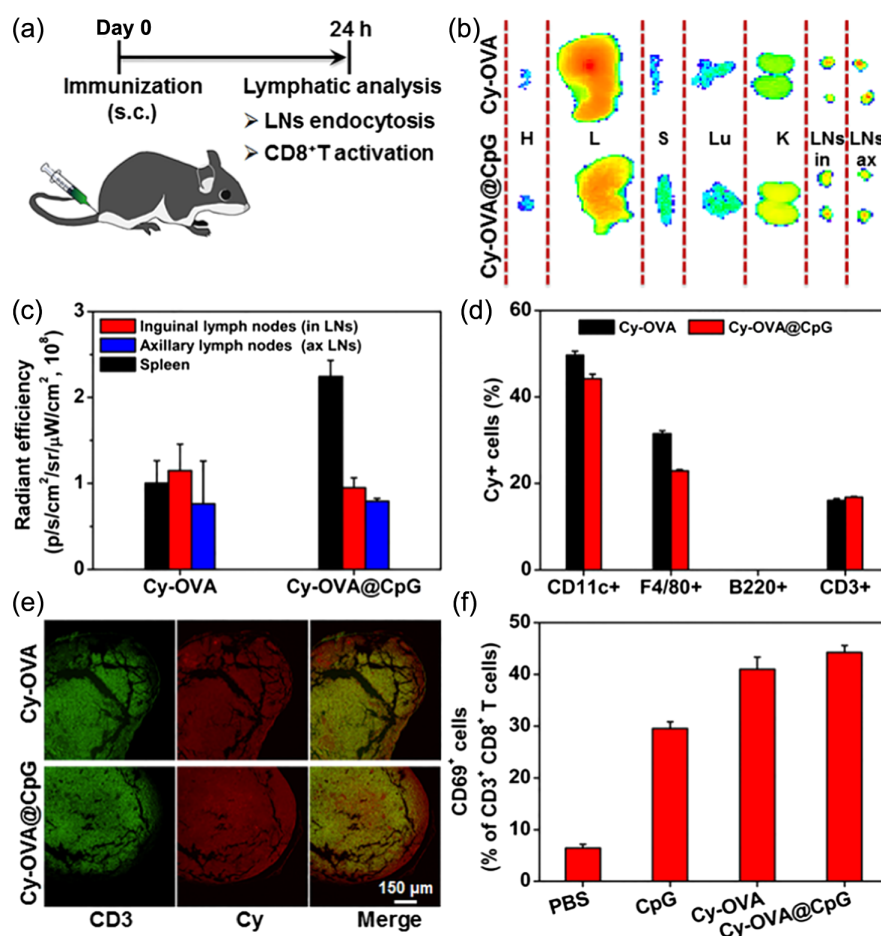


Figure 4 | *In vivo* lymphatic homing and immune responses of nanovaccines. (a) Schematic diagram of lymphatic analysis. (b) After 24 h, ex vivo NIR fluorescence imaging of heart, liver, spleen, lung, kidney, and LNs of the mice subcutaneously injected with nanovaccines. (c) The quantitative distribution of nanovaccines in the primary secondary lymphoid tissues, including spleen, axillary, and inguinal nodes. (d) The distribution of nanovaccines in various lymphocytes was analyzed by flow cytometry. (e) The distribution of nanovaccines and CD3⁺ T cells in LNs was analyzed by immunofluorescence. (f) The expression level of specific marker CD69 on the surface of CD8⁺ T cells.

Cy-OVA, were found to distribute in the major organs including heart, liver, spleen, lung, kidney, and LNs of mice at 24 h postinjection (Figure 4b). Although the signals of Cy-OVA@CpG and Cy-OVA are rather comparable from both axillary and inguinal nodes (Figure 4c) the signal of the former from spleen is twice as high as that of the latter. To further quantify the uptake of the nanovaccines by cells of specific types in the primary and secondary lymphoid tissues, LNs were extracted and dissected into a single cell suspension for flow cytometry analysis. Figure 4d reveals that LN accumulation of the nanovaccines is strongly associated with CD11c⁺ DCs (40–50%), F4/80⁺ macrophages (20–30%), and CD3⁺ T cells (~15%), with negligible contributions from B220⁺ B cells.

The following histological immunofluorescence analysis of draining LNs implied that the Cy-OVA@CpG nanovaccine and its control, Cy-OVA nanoantigen, are mainly accumulated in the region where CD3⁺ T cells are

populated, as shown in Figure 4e. The quantified results in Figure 4f indicate that the nanovaccines can further activate CD3⁺ T cells to differentiate into CD8⁺ T cells that specifically express CD69 marker on the cell surface. Specifically, approximately 45% of CD3⁺CD8⁺ T cells express CD69 after the mice receive injection of Cy-OVA@CpG, while it is about 42% for the Cy-OVA nanoantigen group, and they both are much higher (~30%) than that for the CpG group. Despite that lymphadenopathy of draining LNs is an indicator for local activity, Cy-OVA@CpG nanovaccines showed greatly reduced systemic inflammation in comparison with free CpG, as indicated by the size variation of spleens harvested from different groups (Supporting Information Figure S5). All these results support that the LN targeting of the Cy-OVA@CpG nanovaccines can effectively induce immune responses while simultaneously showing low systemic side effects.

Immune memory created by the nanovaccines

Owing to the immune memory effect of the lymphocytes trained by vaccine, the memory T cells can be activated rapidly upon restimulation.³⁷ Inspired by the efficient lymphatic homing and effective activation of CD8⁺ T cells, we further evaluated the ability of Cy-OVA@CpG in generating OVA-specific cytotoxic T lymphocyte (CTL) response with the detailed procedures given in Figure 5a. The spleen of naive mouse was harvested to get splenocyte suspension. Then, half of the splenocytes was pulsed with free OVA for 2 h followed by weak staining with 0.5 mM carboxyfluorescein diacetate succinimidyl ester (CFSE), while the second half of the splenocytes was not pulsed but subjected to high-staining with 5 mM CFSE. Then, the resulting cells were mixed and injected intravenously into immunized mice 7 days postvaccination. After 16 h, the blood was collected, lysed, and subjected to flow cytometry analysis to determine the numbers of OVA-pulsed and -unpulsed cells for further estimating the OVA-specific splenocyte killing activity. The results shown in Figures 5b and 5c clearly reveal that Cy-OVA@CpG nanovaccines give rise to the highest OVA-specific killing activity of splenocytes, approximately three times stronger than that achieved with Cy-OVA nanoantigens, suggesting that nanovaccines can remarkably enhance the OVA-specific CTL response.

The OVA-specific CD8⁺ T cell response is generally associated with the major histocompatibility complex (MHC) class I-dependent antigen presentation pathway in the immune memory effect,³ and the MHC class I molecules expressed on splenocytes regulate the selection of CD8⁺ T cells during T cell activation. To clarify the mechanism of cellular immunity and show the durability of the immune memory effect, the spleens were harvested on the 45th day from when the mice received two booster immunizations for extracting splenocytes with the detailed procedures given in Figure 5d. Then, the percentage of OVA-specific CD8⁺ T cells in CD3⁺CD8⁺ T cells from the whole splenic lymphocytes was determined with flow cytometry via SIINFEKL-MHC I pentamer staining. The results in Figure 5e and Supporting Information Figure S6 show that the percentage of OVA-specific CD8⁺ T cells in mice immunized with Cy-OVA@CpG increases by a factor of ~3 in comparison with that of the phosphate-buffered saline (PBS) group and is much higher than that (~2) achieved with the Cy-OVA nanoantigens, while the CpG group presents no change in reference to the PBS group. These results demonstrate that the coadministration of OVA and CpG in the form of nanovaccines successfully induce robust immunological memory in vivo.

Once immune memory is created, memory T cells will generate a strong response even under low-level antigen restimulation.⁴ To verify such responsiveness, the

splenocytes obtained from mice vaccinated with Cy-OVA@CpG were restimulated with OVA (15 μg mL⁻¹) ex vivo for 5 h, and then the percentage of OVA-specific CD8⁺ T cells expressing intracellular marker IFN-γ was determined by flow cytometry. As shown in Supporting Information Figure S7 and Figure 5f, the nanovaccine presents the highest level of IFN-γ expressing CD8⁺ T cells, that is, 1.3 ± 0.3% among all groups of mice receiving PBS, CpG, Cy-OVA, and Cy-OVA@CpG. Meanwhile, the levels of extracellular cytokines in the supernatants of OVA-specific CD8⁺ T cells restimulated with OVA (15 μg mL⁻¹/48 h) were also determined by the MSD method. The results shown in Figures 5g and 5h reflect that the expression levels of IFN-γ and TNF-α in memory CD8⁺ T cells of Cy-OVA@CpG immunized mice are the highest among all groups and approximately 2.3 and 1.9 times higher than that recorded from the corresponding Cy-OVA nanoantigens, and 10.2 and 4.3 times higher than those of the corresponding PBS control groups, respectively. Therefore, it can be concluded that the DC-specific nanovaccines can potentially create strong and robust immunologic memory against the subsequent tumor challenges.

In vivo antitumor performance of nanovaccines

To investigate the preventive effect of the nanovaccines against tumor, C57/BL6 mice (*n* = 8) were immunized subcutaneously once a week for 3 weeks, with PBS, CpG, and Cy-OVA serving as controls. Then, B16F10-OVA⁺ melanoma cells (6 × 10⁵) were inoculated subcutaneously on the right back of mice 15 days after the first immunization (Figure 6a). The tumor growth was carefully monitored by recording the temporal tumor size. As shown in Figures 6b and 6c, the tumors in the PBS group appear 1 week after inoculation and then gradually grow bigger with the highest growth rate. Well in accordance with literature results,^{9,38,39} CpG presents a certain level of immune response against tumor growth, characterized by a weak tumor inhibition effect, yet the tumor remains massive 3 weeks postinoculation of the tumor cells. The Cy-OVA nanoantigens present very strong tumor inhibition effect with tumor size decreased by a factor of 4.3 in comparison with PBS. In contrast, the tumor growth in mice immunized with Cy-OVA@CpG nanovaccines is remarkably suppressed with tumor size decreased by a factor of 82.5.

The tumor inhibition effect of the Cy-OVA@CpG nanovaccines may result from a series of immune responses including the DCs' maturation and the migration of nanovaccines to the lymphatic system, OVA-specific CD8⁺ T cell activation, and ultimately tumor inhibition.⁴⁰ To clarify the corresponding mechanisms in vivo, all immunized mice were sacrificed on the 35th day after the first immunization, and the levels of different cytokines in the

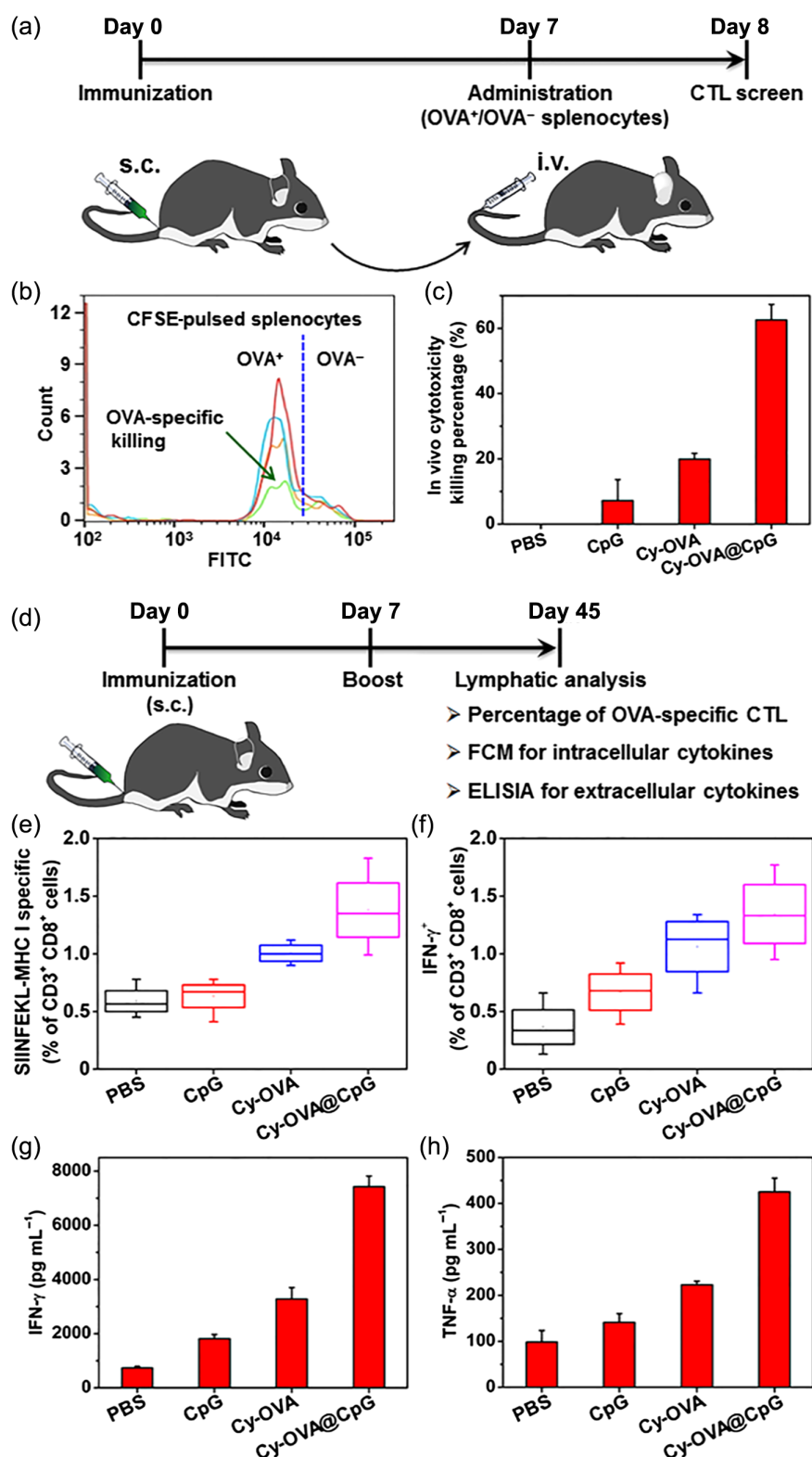


Figure 5 | The immune memory effect of the lymphocyte stimulated with nanovaccines. (a) Schematic diagram of short-term immune memory effect analysis. (b) Flow cytometry for OVA-specific spleen lymphocyte analysis. (c) The quantitative OVA-specific splenocyte killings in each group. (d) Schematic diagram of long-term immune memory effect analysis. (e) Flow cytometry with SIINFEKL-MHC I pentamer staining for the proportion of OVA-specific CD8⁺ T cells in the CD3⁺CD8⁺ T cells. (f) Flow cytometry of intracellular IFN- γ of CD8⁺ T cells. (g) Enzyme-linked immunosorbent assay (ELISA) of extracellular IFN- γ in memory CD8⁺ T cells. (h) ELISA of extracellular TNF- α in memory CD8⁺ T cells.

DOI: 10.31635/ccschem.021.202000670

Corrected Citation: CCS Chem. 2022, 4, 1238-1250

Previous Citation: CCS Chem. 2021, 3, 1328-1340

Link to VoR: <https://doi.org/10.31635/ccschem.021.202000670>

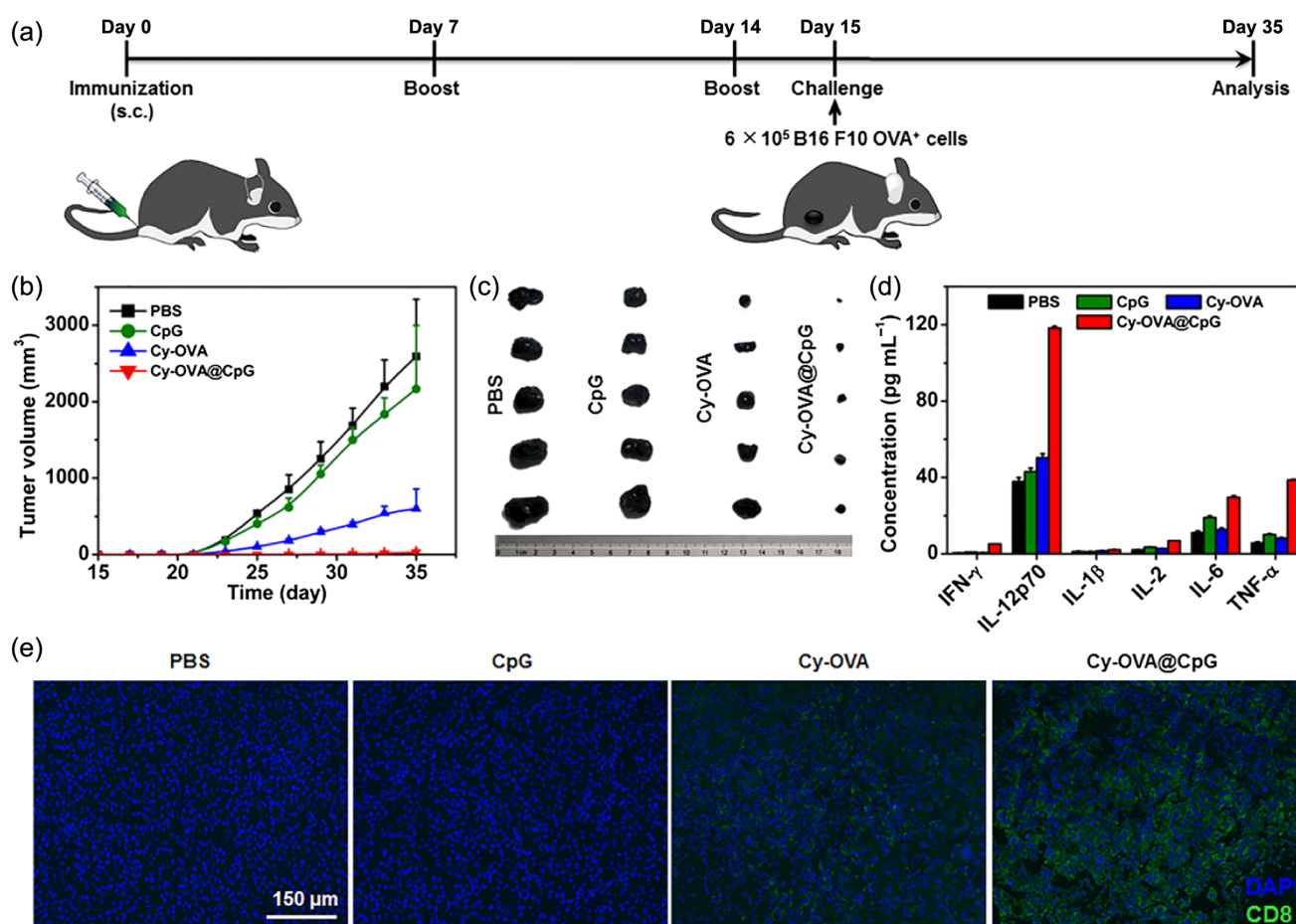


Figure 6 | *In vivo* antitumor immune responses of nanovaccines. (a) Schematic diagram of antitumor immune responses of nanovaccines. (b) Tumor growth inhibition profiles of the mice bearing B16F10 OVA⁺ tumor immunized with nanovaccines. (c) Photographs of the tumors extracted from the mice bearing 4T1 tumor at the end of the above experiment. (d) MSD based on electrochemiluminescence technology for the sensitive detection of specific cytokines in the serum of the mice-bearing B16F10 OVA⁺ tumor immunized with nanovaccines. (e) Fluorescence immunohistochemical analysis for cytotoxic CD8⁺ T cells in the tumors of the mice-bearing B16F10 OVA⁺ tumor immunized with nanovaccines.

blood were analyzed. T helper type 1 (Th1) cytokines including TNF- α , IL-6, IL-2, IL-1 β , IL-12p70, and IFN- γ are highly secreted in mice immunized with the nanovaccines (Figure 6d). Specifically, the serum levels of TNF- α and IFN- γ , the most typical cytokine of the Th1 subtypes, drastically increase by factors of 6.8 and 8.5, respectively, when compared with the PBS group. In addition, the levels of other types of cytokines secreted by nanovaccine-immunized mice also increase by factors of 2.6 (IL-6), 3.3 (IL-2), 1.2 (IL-1 β), and 3.1 (IL-12p70) in comparison with those of the PBS group, which in return promotes the proliferation of cytotoxic CD8⁺ T cells.

All above results indicate that the cytotoxic CD8⁺ T cells can effectively be primed by the nanovaccines, which is essential for suppressing the tumor growth.⁴¹ To further provide direct proof on this hypothesis, the tumors were extracted and then subjected to pathological immunofluorescence analysis. Figure 6e shows that

the signal of CD8⁺ T cells infiltrating into tumors is hardly observable from the PBS and CpG groups. Although the Cy-OVA group presents a certain level of CD8⁺ T cells, the nanovaccine group apparently exhibits the highest level of CD8⁺ T cells, which strongly supports the above mechanism and explains well the excellent antitumor effect of the Cy-OVA@CpG nanovaccine.

Systemic circulation of vaccines can also trigger immunity responses to exert strong antitumor effects.^{42,43} Since CpG possesses a sugar-phosphate backbone, it may exhibit specific targeting ability toward malignant bone tumors. Therefore, the immune response was evaluated on an orthotopic K7M2 osteosarcoma model after the nanovaccines were intravenously administrated. *In vivo* NIR fluorescence imaging (Supporting Information Figure S8a) reveals that the Cy-OVA@CpG nanovaccines exhibit higher tumor binding affinity *in vivo* than the corresponding nanoantigens, supporting the positive

contribution of the CpG moieties. It was further confirmed that the Cy-OVA@CpG nanovaccines can inhibit well the tumor growth after three booster immunizations (Supporting Information Figures S8b and S8c). As the typical cytokines of Th1 subtypes, TNF- α and IFN- γ were also expressed in the serum of Cy-OVA@CpG nanovaccines-immunized K7M2 and B16-OVA tumor-bearing mice with higher levels, as shown in Supporting Information Figure S9, than in the serum of the control groups of mice. Despite these positive immune responses, the prevention of the tumor recurrence failed through the intravenous delivery of the nanovaccines. These results suggest that DCs-nanovaccines can prime T-cell immunity regardless of the route of administration, but the quality of the OVA-specific response is inconsistent and the subcutaneous injection is apparently superior to the intravenous delivery with respect to tumor growth inhibition and recurrence.

Finally, the safety of the nanovaccines is also a paramount issue with respect to clinical translation. The major organs of mice from each group were collected for pathological analysis. Supporting Information Figure S10 shows that no significant difference between the Cy-OVA@CpG group and its control groups is observed from the tissues of the major organs stained with hematoxylin and eosin, indicating that the nanovaccines have no obvious acute toxicity and hardly induce systemic inflammation.

Conclusion

An innovative OVA/CpG-based nanovaccine for cancer immunotherapy is designed with the following outstanding features, including simultaneous accessibility of both antigen and adjuvant, possession of surface maleimide residues for enhancing DC-specific targeting, and intercalary embedded NIR fluorescent dye for noninvasively monitoring the spatiotemporal trafficking of the nanovaccines in vivo. Both in-depth in vitro and in vivo studies reveal that the Cy-OVA@CpG nanovaccines can sufficiently target and activate the DCs. The effective lymphatic homing of the matured DCs and the consequent priming of CD8⁺ T cells initiate strong tumor-specific T-cell responses that show a robust immune memory effect. Owing to these performances, the Cy-OVA@CpG nanovaccines exhibit remarkable antitumor effects against both tumor growth and tumor recurrence, which can be attributed to the unique nanovaccine structures.

Supporting Information

Supporting Information is available and includes synthesis details of nanoantigen and nanovaccines; DCs phenotypic changes and TLR9 detection in vitro; antigen presentation of DCs in vitro; cytoskeleton staining and

chemotactic ability of DCs; in vivo imaging of nanovaccines and nanovaccines labeled-DCs; LNs tracing of nanovaccines; CD8⁺ T cells activation analysis in LNs; CTL killing assays; antigen presentation and the ability of cytokine release of DCs in vivo; tumor growth inhibition by nanovaccines; and biocompatibility and toxicity.

Conflict of Interest

There is no conflict of interest to report.

Funding Information

This work was supported by National Natural Science Foundation of China (nos. 21874097 and 12075164), National Key Research Program of China (no. 2018YFA0208800), Suzhou Administration of Science and Technology (no. sys2018021), Jiangsu Province's Natural Science Foundation (no. SBK2020041529), Pre-Research Foundation of the Second Affiliated Hospital of Soochow University (no. SDFEYBS1906), the Scientific Research Program for Young Talents of China National Nuclear Corporation and A Priority Academic Program Development of Jiangsu Higher Education Institutions (PAPD). Professor Yubin Ke is grateful to the support by the Youth Innovation Promotion Association, Chinese Academy of Sciences (no. 2020010).

Acknowledgments

SANS measurements were performed on an instrument installed at the China Spallation Neutron Source.

References

1. Finn, O. J. The Dawn of Vaccines for Cancer Prevention. *Nat. Rev. Immunol.* **2018**, *18*, 183–194.
2. Schudel, A.; Francis, D. M.; Thomas, S. N. Material Design for Lymph Node Drug Delivery. *Nat. Rev. Mater.* **2019**, *4*, 415–428.
3. Perez, C. R.; De Palma, M. Engineering Dendritic Cell Vaccines to Improve Cancer Immunotherapy. *Nat. Commun.* **2019**, *10*, 5408.
4. Demaria, O.; Cornen, S.; Daëron, M.; Morel, Y.; Medzhitov, R.; Vivier, E. Harnessing Innate Immunity in Cancer Therapy. *Nature* **2019**, *574*, 45–56.
5. Moyer, T. J.; Kato, Y.; Abraham, W.; Chang, J. Y. H.; Kulp, D. W.; Watson, N.; Turner, H. L.; Menis, S.; Abbott, R. K.; Bhiman, J. N.; Melo, M. B.; Simon, H. A.; Herrera-De la Mata, S.; Liang, S.; Seumois, G.; Agarwal, Y.; Li, N.; Burton, D. R.; Ward, A. B.; Schief, W. R.; Crotty, S.; Irvine, D. J. Engineered Immunogen Binding to Alum Adjuvant Enhances Humoral Immunity. *Nat. Med.* **2020**, *26*, 430–440.
6. Xia, Y.; Xie, Y.; Yu, Z.; Xiao, H.; Jiang, G.; Zhou, X.; Yang, Y.; Li, X.; Zhao, M.; Li, L.; Zheng, M.; Han, S.; Zong, Z.; Meng, X.

- Deng, H.; Ye, H.; Fa, Y.; Wu, H.; Oldfield, E.; Hu, X.; Liu, W.; Shi, Y.; Zhang, Y. The Mevalonate Pathway Is a Druggable Target for Vaccine Adjuvant Discovery. *Cell* **2018**, *175*, 1059-1073.
7. Krieg, A. M. Therapeutic Potential of Toll-Like Receptor 9 Activation. *Nat. Rev. Drug Discov.* **2006**, *5*, 471-484.
8. McWhirter, S. M.; Jefferies, C. A. Nucleic Acid Sensors as Therapeutic Targets for Human Disease. *Immunity* **2020**, *53*, 78-97.
9. Frank, M. J.; Reagan, P. M.; Bartlett, N. L.; Gordon, L. I.; Friedberg, J. W.; Czerwinski, D. K.; Long, S. R.; Hoppe, R. T.; Janssen, R.; Candia, A. F.; Coffman, R. L.; Levy, R. In Situ Vaccination with a TLR9 Agonist and Local Low-Dose Radiation Induces Systemic Responses in Untreated Indolent Lymphoma. *Cancer Discov.* **2018**, *8*, 1258-1269.
10. Pearson, R. M.; Casey, L. M.; Hughes, K. R.; Wang, L. Z.; North, M. G.; Getts, D. R.; Miller, S. D.; Shea, L. D. Controlled Delivery of Single or Multiple Antigens in Tolerogenic Nanoparticles Using Peptide-Polymer Bioconjugates. *Mol. Ther.* **2017**, *25*, 1655-1664.
11. Skakuj, K.; Wang, S.; Qin, L.; Lee, A.; Zhang, B.; Mirkin, C. A. Conjugation Chemistry-Dependent T-Cell Activation with Spherical Nucleic Acids. *J. Am. Chem. Soc.* **2018**, *140*, 1227-1230.
12. Ni, Q.; Zhang, F.; Liu, Y.; Wang, Z.; Yu, G.; Liang, B.; Niu, G.; Su, T.; Zhu, G.; Lu, G.; Zhang, L.; Chen, X. A Bi-Adjuvant Nanovaccine that Potentiates Immunogenicity of Neoantigen for Combination Immunotherapy of Colorectal Cancer. *Sci. Adv.* **2020**, *6*, eaaw6071.
13. Kuai, R.; Ochyl, L. J.; Bahjat, K. S.; Schwendeman, A.; Moon, J. J. Designer Vaccine Nanodiscs for Personalized Cancer Immunotherapy. *Nat. Mater.* **2017**, *16*, 489-496.
14. Scheetz, L.; Kadiyala, P.; Sun, X.; Son, S.; Hassani Najafabadi, A.; Aikins, M.; Lowenstein, P. R.; Schwendeman, A.; Castro, M. G.; Moon, J. J. Synthetic High-Density Lipoprotein Nanodiscs for Personalized Immunotherapy Against Gliomas. *Clin. Cancer Res.* **2020**, *26*, 4369-4380.
15. Hong, X.; Zhong, X.; Du, G.; Hou, Y.; Zhang, Y.; Zhang, Z.; Gong, T.; Zhang, L.; Sun, X. The Pore Size of Mesoporous Silica Nanoparticles Regulates Their Antigen Delivery Efficiency. *Sci. Adv.* **2020**, *6*, eaaz4462.
16. Radovic-Moreno, A. F.; Chernyak, N.; Mader, C. C.; Nallagatla, S.; Kang, R. S.; Hao, L.; Walker, D. A.; Halo, T. L.; Merkel, T. J.; Rische, C. H.; Anantatmula, S.; Burkhart, M.; Mirkin, C. A.; Gryaznov, S. M. Immunomodulatory Spherical Nucleic Acids. *Proc. Natl. Acad. Sci. U. S. A.* **2015**, *112*, 3892-3897.
17. Harari, A.; Graciotti, M.; Bassani-Sternberg, M.; Kandalaft, L. E. Antitumour Dendritic Cell Vaccination in a Priming and Boosting Approach. *Nat. Rev. Drug Discov.* **2020**, *19*, 635-652.
18. Liu, H.; Moynihan, K. D.; Zheng, Y.; Szeto, G. L.; Li, A. V.; Huang, B.; Van Egeren, D. S.; Park, C.; Irvine, D. J. Structure-Based Programming of Lymph-Node Targeting in Molecular Vaccines. *Nature* **2014**, *507*, 519-522.
19. Martin, J. D.; Cabral, H.; Stylianopoulos, T.; Jain, R. K. Improving Cancer Immunotherapy Using Nanomedicines: Progress, Opportunities and Challenges. *Nat. Rev. Clin. Oncol.* **2020**, *17*, 251-266.
20. Riley, R. S.; June, C. H.; Langer, R.; Mitchell, M. J. Delivery Technologies for Cancer Immunotherapy. *Nat. Rev. Drug Discov.* **2019**, *18*, 175-196.
21. Kooreman, N. G.; Ransohoff, J. D.; Wu, J. C. Tracking Gene and Cell Fate for Therapeutic Gain. *Nat. Mater.* **2014**, *13*, 106-109.
22. Nishino, M.; Hatabu, H.; Hodi, F. S. Imaging of Cancer Immunotherapy: Current Approaches and Future Directions. *Radiology* **2018**, *290*, 9-22.
23. Wculek, S. K.; Cueto, F. J.; Mujal, A. M.; Melero, I.; Krummel, M. F.; Sancho, D. Dendritic Cells in Cancer Immunology and Immunotherapy. *Nat. Rev. Immunol.* **2020**, *20*, 7-24.
24. Tian, R.; Ke, C.; Rao, L.; Lau, J.; Chen, X. Multimodal Stratified Imaging of Nanovaccines in Lymph Nodes for Improving Cancer Immunotherapy. *Adv. Drug Deliv. Rev.* **2020**, *161-162*, 145-160.
25. Lindsay, K. E.; Bhosle, S. M.; Zurla, C.; Beyersdorf, J.; Rogers, K. A.; Vanover, D.; Xiao, P.; Araing, M.; Shirreff, L. M.; Pitard, B.; Baumhof, P.; Villinger, F.; Santangelo, P. J. Visualization of Early Events in mRNA Vaccine Delivery in Non-Human Primates via PET-CT and Near-Infrared Imaging. *Nat. Biomed. Eng.* **2019**, *3*, 371-380.
26. Wang, H.; Mooney, D. J. Biomaterial-Assisted Targeted Modulation of Immune Cells in Cancer Treatment. *Nat. Mater.* **2018**, *17*, 761-772.
27. van der Meel, R.; Sulheim, E.; Shi, Y.; Kiessling, F.; Mulder, W. J. M.; Lammers, T. Smart Cancer Nanomedicine. *Nat. Nanotechnol.* **2019**, *14*, 1007-1017.
28. Wang, Y.; Sun, Z.; Chen, Z.; Wu, Y.; Gu, Y.; Lin, S.; Wang, Y. In Vivo Photoacoustic/Single-Photon Emission Computed Tomography Imaging for Dynamic Monitoring of Aggregation-Enhanced Photothermal Nanoagents. *Anal. Chem.* **2019**, *91*, 2128-2134.
29. de Titta, A.; Ballester, M.; Julier, Z.; Nembrini, C.; Jeanbart, L.; van der Vlies, A. J.; Swartz, M. A.; Hubbell, J. A. Nanoparticle Conjugation of CpG Enhances Adjuvancy for Cellular Immunity and Memory Recall at Low Dose. *Proc. Natl. Acad. Sci. U. S. A.* **2013**, *110*, 19902-19907.
30. Watkins, E. A.; Hubbell, J. A. Designing Biofunctional Immunotherapies. *Nat. Rev. Mater.* **2019**, *4*, 350-352.
31. Sahaf, B.; Heydari, K.; Herzenberg, L. A.; Herzenberg, L. A. Lymphocyte Surface Thiol Levels. *Proc. Natl. Acad. Sci. U. S. A.* **2003**, *100*, 4001-4005.
32. Stephan, M. T.; Moon, J. J.; Um, S. H.; Bershteyn, A.; Irvine, D. J. Therapeutic Cell Engineering with Surface-Conjugated Synthetic Nanoparticles. *Nat. Med.* **2010**, *16*, 1035-1041.
33. Huang, B.; Abraham, W. D.; Zheng, Y.; Bustamante López, S. C.; Luo, S. S.; Irvine, D. J. Active Targeting of Chemotherapy to Disseminated Tumors Using Nanoparticle-Carrying T Cells. *Sci. Transl. Med.* **2015**, *7*, 291ra94.
34. Jakubzick, C. V.; Randolph, G. J.; Henson, P. M. Monocyte Differentiation and Antigen-Presenting Functions. *Nat. Rev. Immunol.* **2017**, *17*, 349-362.
35. Obermajer, N.; Urban, J.; Wieckowski, E.; Muthuswamy, R.; Ravindranathan, R.; Bartlett, D. L.; Kalinski, P. Promoting the Accumulation of Tumor-Specific T Cells in Tumor Tissues by

- Dendritic Cell Vaccines and Chemokine-Modulating Agents. *Nat. Protoc.* **2018**, *13*, 335–357.
36. Xi, X.; Ye, T.; Wang, S.; Na, X.; Wang, J.; Qing, S.; Gao, X.; Wang, C.; Li, F.; Wei, W.; Ma, G. Self-Healing Microcapsules Synergetically Modulate Immunization Microenvironments for Potent Cancer Vaccination. *Sci. Adv.* **2020**, *6*, eaay7735.
37. Luo, M.; Wang, H.; Wang, Z.; Cai, H.; Lu, Z.; Li, Y.; Du, M.; Huang, G.; Wang, C.; Chen, X.; Porembka, M. R.; Lea, J.; Frankel, A. E.; Fu, Y.-X.; Chen, Z. J.; Gao, J. A STING-Activating Nanovaccine for Cancer Immunotherapy. *Nat. Nanotechnol.* **2017**, *12*, 648–654.
38. Alam, I. S.; Mayer, A. T.; Sagiv-Barfi, I.; Wang, K.; Vermesh, O.; Czerwinski, D. K.; Johnson, E. M.; James, M. L.; Levy, R.; Gambhir, S. S. Imaging Activated T Cells Predicts Response to Cancer Vaccines. *J. Clin. Invest.* **2018**, *128*, 2569–2580.
39. Sagiv-Barfi, I.; Czerwinski, D. K.; Levy, S.; Alam, I. S.; Mayer, A. T.; Gambhir, S. S.; Levy, R. Eradication of Spontaneous Malignancy by Local Immunotherapy. *Sci. Transl. Med.* **2018**, *10*, eaan4488.
40. Zhu, G.; Lynn, G. M.; Jacobson, O.; Chen, K.; Liu, Y.; Zhang, H.; Ma, Y.; Zhang, F.; Tian, R.; Ni, Q.; Cheng, S.; Wang, Z.; Lu, N.; Yung, B. C.; Wang, Z.; Lang, L.; Fu, X.; Jin, A.; Weiss, I. D.; Vishwasrao, H.; Niu, G.; Shroff, H.; Klinman, D. M.; Seder, R. A.; Chen, X. Albumin/Vaccine Nanocomplexes that Assemble in Vivo for Combination Cancer Immunotherapy. *Nat. Commun.* **2017**, *8*, 1954.
41. Kim, Y.; Kang, S.; Shin, H.; Kim, T.; Yu, B.; Kim, J.; Yoo, D.; Jon, S. Sequential and Timely Combination of a Cancer Nanovaccine with Immune Checkpoint Blockade Effectively Inhibits Tumor Growth and Relapse. *Angew. Chem. Int. Ed.* **2020**, *59*, 14628–14638.
42. Ols, S.; Yang, L.; Thompson, E. A.; Pushparaj, P.; Tran, K.; Liang, F.; Lin, A.; Eriksson, B.; Hedestam, G. B. K.; Wyatt, R. T.; Lore, K. Route of Vaccine Administration Alters Antigen Trafficking but Not Innate or Adaptive Immunity. *Cell Rep.* **2020**, *30*, 3964–3971.
43. Hegde, P. S.; Chen, D. S. Top 10 Challenges in Cancer Immunotherapy. *Immunity* **2020**, *52*, 17–35.